Zuse Institute Berlin

Takustr. 7
14195 Berlin
Germany

YULIA ZHUKOVA, CHRISTIAN HIEPEN, PETRA KNAUS,
MARC OSTERLAND, STEFFEN PROHASKA,
JOHN W.C. DUNLOP, EKATERINA V. SKORB,
PETER FRATZL

The role of titanium surface nanotopography on preosteoblast morphology, adhesion and migration[1]

[1]The manuscript will also appear in revised form in Advanced Healthcare Materials.

ZIB Report 17-06 (February 2017)

Zuse Institute Berlin
Takustr. 7
D-14195 Berlin

Telefon: +49 30-84185-0
Telefax: +49 30-84185-125

e-mail: bibliothek@zib.de
URL: http://www.zib.de

ZIB-Report (Print) ISSN 1438-0064
ZIB-Report (Internet) ISSN 2192-7782

The role of surface nanotopography on preosteoblast morphology, adhesion and migration

*Yulia Zhukova, Christian Hiepen, Petra Knaus, Marc Osterland, Steffen Prohaska, John W. C. Dunlop, Ekaterina V. Skorb, Peter Fratzl**

Y. Zhukova, Dr. J. W. C. Dunlop, Dr. E. V. Skorb, Prof. P. Fratzl
Department of Biomaterials, Max Planck Institute of Colloids and Interfaces, 14476 Potsdam-Golm, Germany
E-mail: peter.fratzl@mpikg.mpg.de
Dr. C. Hiepen, Prof. P. Knaus
Institute for Chemistry and Biochemistry, Freie Universität Berlin, 14195 Berlin, Germany
M. Osterland, Dr. S. Prohaska
Zuse Institute Berlin, 14195 Berlin, Germany

Keywords: titanium, metal, nanotopography, interface, cell adhesion, migration

Surface structuring of titanium-based implants with appropriate nanotopographies can significantly modulate their impact on the biological behavior of cells populating these implants. Implant assisted bone tissue repair and regeneration require functional adhesion and expansion of bone progenitors. The surface nanotopography of implant materials used to support bone healing and its effect on cell behavior, in particular cell adhesion, spreading, expansion, and motility, is still not clearly understood. The aim of this study is to investigate preosteoblast proliferation, adhesion, morphology, and migration on different titanium materials with similar surface chemistry, but distinct nanotopographical features. Sonochemical treatment and anodic oxidation were employed to fabricate disordered – mesoporous titania (TMS), and ordered – titania nanotubular (TNT) topographies respectively. The morphological evaluation revealed a surface dependent shape, thickness, and spreading of cells owing to different adherence behavior. Cells were polygonal-shaped and well-spread on glass and TMS, but displayed an elongated fibroblast-like morphology on TNT surfaces. The cells on glass however, were much flatter than on nanostructured surfaces. Both nanostructured surfaces impaired cell adhesion, but TMS was more favorable for cell growth

due to its support of cell attachment and spreading in contrast to TNT. Quantitative wound healing assay in combination with live-cell imaging revealed that cells seeded on TMS surfaces migrated in close proximity to neighboring cells and less directed when compared to the migratory behavior on other surfaces. The results indicate distinctly different cell adhesion and migration on ordered and disordered titania nanotopographies, providing important information that could be used in optimizing titanium-based scaffold design to foster bone tissue growth and repair.

1. Introduction

Recent advances in material research have gained an increased knowledge on the role of the extracellular environment for tissue repair and regeneration processes.[1-3] The physical and chemical cues presented by the extracellular environment have been shown to directly impact cell behavior such as proliferation, adherence and migration. Little is known on the impact of topography of the extracellular environment on bone progenitor proliferation, adhesion and migration. To date, titanium and its alloys find wide application in regenerative medicine representing clinically relevant implant materials, which need further improvement for enhancement of healing and tissue regeneration. Here we aim here at understanding the impact of extracellular topography on bone progenitor-cell behavior by using smart functional titanium-based materials. [4-6]

Several studies using surface structuring approaches demonstrate that cells respond to nanotopography.[7-11] Interactions between biomaterials and host tissues are controlled by nanoscale features such as: (1) cells grow on nanostructured extracellular matrices; (2) biological events such as signaling occur at the nanometric level; (3) adsorbed proteins and their aggregates are a few nanometers in dimension. [12]

Physical cues of the extracellular space such as stiffness and topography are most-likely sensed by the cells focal contact points or focal adhesions. Selhuber-Unkel *et al.*[7] have shown that the spacing between gold nanopatterns on glass substrates determines the strength

of cell adhesion. These results suggest that "cells can amplify small differences in adhesive cues to large differences in cell adhesion strength". Oh *et al.*[9] showed that titania nanotube diameter can strongly alter the differentiation pathway of human mesenchymal stem cells (hMSC). They found that larger (≈70 to 100 nm) nanotubes induced the differentiation of stem cells into osteoblast-like cells due to the induced cytoskeletal stress and dramatic cell elongation.

Titanium is a common material used in dental and orthopaedic implants due to its inertness and high mechanical strength. A variety of surface modification strategies can be employed to titanium-based implants to enhance osseointegration.[13-16] Straight-forward surface treatments of titanium and its alloys can be divided into three main groups: mechanical, chemical, and physical methods[13]. These methods are used either individually or in combination with each other, and cause the formation of different nanotopographies. Major disadvantages of mechanical and physical methods are: they are expensive, time consuming, or difficult to apply for large scale implant production.[17] In contrast, chemical treatments seem to be attractive for large-scale manufacturing, because they provide uniform access of the reactive substance to all surfaces, which could be applied for multifaceted devices with complex geometries such as dental screws and cardiovascular stents. However, the majority of chemical methods modify not only topography, but also other surface features, such as chemical composition,[18] wettability,[19] crystallinity,[20] and adsorption ability.[21] These surface observables can also modulate cell behavior [20, 22-24] (for more information about surface modification strategies and cellular recognition of these surfaces see these review papers[25-26]), and it is difficult to distinguish, which factor leads to the respective cell response.

In this study, high-intensity ultrasound treatment (HIUS) was used in combination with alkali-treatment to gain controllable surface nanostructuring. The method allows fast production and controllable modification of mesoporous titania (TMS).[27] The major advantage of this

technique is that modification can be made on bulk titanium surfaces, important for cost-efficient fabrication. Moreover, active OH-groups formed during the preparation procedure allow for an effective encapsulation of relevant bioactive molecules.[28]

We have recently reported on the response of C2C12 cells to mesoporous titania and titania nanotubes.[29] Titania nanotubes is a well-studied material,[30] produced by anodic oxidation which leads to the formation of TiO_2 nanotube arrays. We observed that the nanostructure of the material has an impact on the osteogenic differentiation, whereas it only moderately affects myogenic differentiation. Therefore, we used here two different nanotopographies: disordered – mesoporous titania, and ordered – titania nanotubes, and studied their effect on cell behavior. Moreover, we investigated for the first time cell migration characteristics of osteoblast-like MC3T3-E1 cells together with cell number, proliferation and adhesion on mesoporous titania and titania nanotubular surfaces.

2. Results and Discussion

2.1. Physicochemical Properties Analysis

To investigate the physicochemical properties of the substrates, scanning electron microscopy (SEM), atomic force microscopy (AFM), and contact angle measurements were performed (**Figure 1**). The surface topography was examined using SEM. Figure 1A illustrates SEM of the titania surface nanotopographies produced by sonochemical treatment and anodic oxidation. The mesoporous titania (TMS) produced by HIUS is a disordered irregular (average pore diameter is *approximately* 70 nm) porous TiO_2 layer. Anodization leads to the formation of TiO_2 nanotube arrays (TNT) with a regular pore diameter of *approximately* 70 nm. As a control either glass or untreated metal was used. A more detailed investigation of surface characteristics is shown in Kopf *et al*.[29] The surface roughness was quantified by AFM (Figure 1 B, C). All surfaces possess nanoscale surface roughness. The arithmetic mean surface roughness (R_a) of the modified surfaces exhibited values of more than 20 nm for nanostructured surfaces and less than 5 nm for unmodified surfaces. The wettability of the

surfaces was quantified by contact angle measurement (**Figure S1**). All surfaces were determined to have contact angles less than 65°, denoting hydrophilicity.[31] Both surface modifications showed very low contact angles, lower than 10°, thereby indicating their highly hydrophilic nature.

Moreover, to estimate the level of nanotopography disorder, Fast Fourier Transform (FFT) measurements were performed on SEM images of mesoporous and nanotubular titania surfaces (**Figure S2**). For this purpose, the SEM micrographs (Figure S2a-b) were firstly binarized (Figure S2c-d), and then FFT measurement was performed twice (Figure S2e-h), followed by the radial integration of the processed image. Final radial profile plot (Figure S2i) depicts smooth and periodic plots for TMS and TNT, respectively. These data indicate the amorphous disordered nature of TMS and periodic ordered nature of TNT.

Thus, both nanostructured surfaces have comparable nanoscale surface roughness and high wettability, but different nanotopographies. Having found that the substrates are biocompatible with similar surface chemistry, we were prompted to perform biological experiments aiming to determine a role of nanotopography in modulation of cell behavior. Biological studies include investigation of cell growth parameters such as proliferation, morphology, adhesion, and cell migration.

2.2. Cell Proliferation

To estimate MC3T3-E1 cell proliferation on surfaces, the density of adhered cells was calculated at 3 and 24 hours after seeding (**Figure 2**). As Figure 2A depicts after 3 hours, the seeded cells populated TMS and glass surfaces with comparable densities (near 5 cells×mm^{-2}), less cells were presented on TNT. However, the effect of nanotopography on cell proliferation was mild at 3 hours (Figure 2B). Considering the density of cells after 3 and 24 hours (Figure 2B), TNT surface slowed down cell proliferation, whereas glass and TMS supported it. As previously described in Biggs *et al*,[32] anchorage-dependent growth of preosteoblasts requires extracellular matrix (ECM) anchorage for efficient proliferation and differentiation. Thus, the

inhibited cell proliferation could be caused by the relatively weak cell adhesion on TNT. To further confirm this suggestion, we performed experiments investigating cell adhesion, described later.

2.3. Cell Morphology

In addition to the different cell densities, we found distinct cell morphologies presented on surfaces (Figure 2C). Three cell morphologies were revealed during the observations: (1) cells with multidirectional protrusions indicating protrusive cell behavior in all directions; (2) elongated cells with a fibroblast-like morphology displaying a distinct leading edge and retracting tail, indicating strong motile behaviour, (3) rounded cells suggesting only mild if any establishment of mature focal contact points with the substratum. Rounded cells are attached but have not begun to spread. All three types of morphologies are seen on all substrates, but in different proportions. The majority of cells grown on TNT are elongated, over 50%. In contrast, cells on TMS and glass have mainly star-like shape, being more than 60%. On each of three substrate types, up to 10% of cells are presented by rounded cells. This finding is statistically significant on 0.001 level. Taken together, the density and shape of adhered cells within 3 hours after seeding are indeed not uniform on different substrates, thereby providing the first evidence of nanotopography induced modulation of cell behavior. Moreover, differences in cell morphology become even more pronounced with the time of cell incubation. To further verify the nanotopography effect on cell morphology, we next performed immunocytochemical staining of the filamentous actin (F-actin) cytoskeleton.

Investigation of F-actin structure and architecture further confirms the nanotopographic effects on cell shape and spreading. The fluorescence micrographs in **Figure 3** illustrate the evolution of cell morphology from 3 hours to 5 days. After 3 hours upon cell seeding (Figure 3A), the adherent cells exerted a rounded or polygonal shape on glass and TMS, which is commonly described as coble-stone like morphology, often seen with resting bone progenitors, and a fibroblast-like shape shape on TNT indicating the formation of unidirectional cellular

protrusions such as lamellipodia[33]. Polarization and protrusion formation was more obvious on TNT compared to the other two substrates and is a hallmark of highly motile cells. After 24 hours (Figure 3B), the adherent cells on all substrates exhibited polygonal shape. However, cells on TNT were more elongated and less spread and still possessed more cellular protrusions. Actin stress fibers tend to align to each other on glass and TMS, whereas on TNT they align in the direction of cell protrusion (Figure 3Ai). Moreover, the cell nuclei on TNT also underwent elongation, whereas the nuclei of cells on glass and TMS remained roundish (Figure 3B, offsets).

To further investigate cell morphology, we next performed SEM of adhered cells (**Figure S3**). SEM micrographs confirm the morphological observations of MC3T3-E1 cells cultured on substrates for 24 hours. After 24 hours of cell adhesion, two cell morphologies could be observed: spread (TMS and Glass) and elongated (TNT). Whereas cells on TMS and glass displayed also with SEM analysis a large amount of spreading and multidirectional protrusions, cells seeded on TNT showed an elongated morphology with clear unidirectional protrusion formation. The high density of the cells cultured for 5 days (Figure 3C) did not allow to accurately observe their morphology. However, according to the calculated number of cell nuclei (Figure 3D), the cell density at this time point followed the order: glass > TMS > TNT. Whereas the cell layer on glass and TMS was comparably dense, it was still possible to observe actin fibers and cell protrusions of single cells on TNT surfaces. Such low density in cell packing is presumably caused by the generally low cell proliferation on TNT described above and their highly elongated morphology. The persistent cell spread on TNT surfaces is also likely caused by relatively little but very mature focal contacts at the leading edges and rear ends of the cells, supporting the idea of mild focal adhesion formation on TNT compared to TMS and Glass. Moreover, the cell thickness after 3 hours was also different (Figure 3E), which can be also one more factor affecting the density of cells packing in the tissue at later stages, e.g. 5 days. Very adherent cells on glass are less thick than on nanostructured titania

surfaces. Surprisingly, mildly adherent cells on TNT had a thickness comparable to the thickness on glass, and cells on TMS had the highest thickness.

Thus, preosteoblasts tended to have specific morphology, thickness, and shape on the substrates, thereby indicating nanotopography induced modulation of cell morphology. Notably, this observation was true for different time points of cell adhesion, after 3 hours, 24 hours and 5 days. Already after 3 hours, cells cultured on glass and TMS possessed numerousprotrusions, which developed homogeneously along the cell periphery, leading to the development of multidirectional protrusions. Cellular protrusions such as filopodia and lamellipodia are actin-rich protrusions that allow the cells to probe the surface while searching for the positions where they can make focal contacts.[12] A continuous "treadmiling-like" stabilization and de-stabilization of these focal contact points within cellular protrusions is prerequisite for cells to move forward.[34] Consistent with previous studies, [35] cells cultured on TNT possessed polarized morphology, characteristic for a migrating cell: leading edge of the lamellipodium with protrusions of filopodia and the trailing edge. One plausible explanation for these differences in cell morphology could be the distribution of adsorbed proteins, which could also be modulated by nanotopography. Whereas the cells on glass and TMS had relatively uniform access to proteins due to the homogeneous localization of proteins on the surface, cells on TNT experienced the necessity to elongate in order to find favorable anchorage points. When anchored, filopodia converts to the flat membrane protrusions called lamellipodia.[36] In Figure 3 is a par-excellence example of a lamellipodial cell shape developing on TNT, thereby indicating strongly migrating cells with less focal contact points on TNT than on TMS and Glass.

Moreover, several studies reported elongated cell morphology on TNTs of similar dimensions[33] and fibroblast-like shape on nanotextured titania produced by etching and other methods.[37-39] These cell behaviors are considered to be related to the size of the cell-surface contact[40] and to the amount of adsorbed proteins that can be recognized by integrin

transmembrane receptor. In this study, the diameter of the nanotubes was approx. 60-70 nm, which was reported to prevent integrin clustering.[33] Such spacing provided protein distribution ineffective for focal contact formation, and the cells had to extend their filopodia in order to find more adsorbed proteins.[41-42] Importantly, TMS has a similar pore diameter, but does not induce elongated morphology and low density of attached cells like on TNT. A possible reason could be a distribution of pore diameter. Although TMS nanotopography is characterized by the similar pore diameter, its distribution is much more irregular than of TNT,[29] which seems to be more favorable for cell attachment and spreading.

2.4. Cell Adhesion

To further investigate the role of surface nanotopography in modulation of cell behavior, we next analysed cell adhesion on the substrates. For this purpose, MC3T3-E1 cells following three hours of incubation on glass and nanostructured titanium substrates were examined by confocal laser scanning microscopy focussing on two intracellular structures, the F-actin and its anchorage points, the focal adhesions (shown by immunocytochemical staining of the ubiquitously expressed focal adhesion marker protein Vinculin) (**Figure 4**). Figure 4A presents the micrographs of double-stained MC3T3-E1 cells, where the green and red areas show F-actin fibers (stained with phalloidin Alexa488) and Vinculin (stained with anti-Vinculin Antibody coupled to Alexa594), respectively.

The microscopy images of single cells in Figure 4B illustrate the focal contact points of MC3T3-E1 cells after 3 hours' adhesion. In line with our previous observations, cells on glass and TMS surface are well spread; one can easily observe quite large amount of actin fibers spreading in multiple directions. In contrast, cells attached to TNT are less spread and start forming more elongated morphology with cellular protrusions of the polarized cell well; actin stress fibers tend to align to each other in the direction of cell protrusion suggesting a motile state.

To estimate cell adhesion on the substrates, various parameters were quantified such as cell area (Figure 4C) and number of vinculin plaques per cell (Figure 4D). The surface nanotopography had an influence on cell spreading. After 3 hours upon cell seeding cell spread area was significantly higher on TMS compared to other surfaces (Figure 4C). In contrast, TNT showed the lowest level of cell spreading. It was also evident that surface nanotopography had an influence on focal contact formation. Although the average area of one focal complex was for all surfaces in the range of 3±2 μm^2 (data not shown), the number of vinculin plaques was significantly higher on glass samples compared to TMS and TNT (Figure 4i).

Notably, although the overall number of vinculin-rich plaques per cell was rather low on both nanostructured surfaces in comparison to glass substrate, TMS performance in cell attachment and morphology was still more favorable than TNT. A plausible explanation is that not only number and area of focal adhesions determines the strength of cell adhesion, but also their localization. In case of glass and TNT, focal adhesions were localized regularly along the cell periphery, whereas on TNT cells were forming adhesion contacts only in proximity to the polarized cell protrusions. Moreover, the strong co-localization of bundled F-actin (as indicated by Phalloidin-staining in green) with Vinculin-rich focal contact points (red) suggests for TMS surfaces a stable but for TNT and glass a rather metastable accumulation of bundle F-actin within focal contact points. It is well known that only mature and long lasting cell adhesions are rich in bundled F-actin, since the F-actin cytoskeleton couples to focal contact points only when they are stable and undergo a slow turn-over (de-stabilization). In contrast, persistence of bundled F-actin in focal contact points is very short lasting, indicating a high turn-over rate observed in migrating and motile cells (TNT and glass).

The directionality of F-actin bundles also indicates towards different directions in cell traction forces. Here the directionality of F-actin bundles on glass and TMS is multidirectional, thereby allowing effective cell spreading. On TNT, stress fibers tend to align and orient with

the length of the cell body, leading to polarization and elongation. The cytoskeletal stresses might also be directly transduced into nuclear function,[43] thereby leading to nuclei elongation on TNT.

Interestingly, compared to TMS, the glass substrate induces stronger cell attachment and bigger amount of focal contacts, but weaker cell spreading. The distribution of adsorbed extracellular matrix proteins on glass seems to be different due to several reasons: surface roughness, surface area, surface geometry and surface chemistry. Although it is still hydrophilic, glass has significantly higher contact angle and lower surface roughness than of the TMS. For example, previous studies reported that very hydrophilic substrates ($\theta<35°$) inhibit the adsorption of serum proteins, causing lower spreading and attachment of human fibroblasts in contrast to the surfaces with moderately wettable surfaces ($\theta=48–62°$).[22]

Taken together, the level of nanotopography (dis)order may have different implications on cell proliferation, morphology and adhesion. Similar to our findings, multiple studies report weak cell attachment on TNT. These observations are also in line with the cell behavior observed on other ordered regular nanofeatures such as nanoposts[44] and nanopits.[45-47] The feature sizes described in these studies are in the range of 80 – 300 nm and higher, which is over a density threshold corresponding to a spacing of integrin-adhesive RGD ligands per unit area, which is approx. 70 nm.[8, 48] Some common effects of ordered nanotopographies with feature sizes exceeding 70 nm on cells include: (1) reduced area of adhesion complexes; (2) increased filopodia; (3) biased orientation; (4) constant traction forces. In contrast, the increased adhesion has been reported on random nanoposts.[49]

2.5. Cell Migration

Cellular morphology, adhesion strength and persistence impact dynamics of cellular motility behavior. To further verify the effect of nanotopography on cell behavior, we asked whether it also affects migratory cell behavior. To our knowledge this is the first study to report *in vitro* migration of MC3T3-E1 cells on mesoporous and nanotubular titania. For this purpose, a

quantitative wound healing assay using live cell microscopy was performed (**Figure 5**). Quantitative wound healing allows commenting on the speed, dynamics and single vs. collective migratory behavior of cells populating a cell free space on the given substrate. This mode of cell behavior is critically important for regenerative processes *in vivo*, as it indicates how fast and by which degree a cell-free implant will be populated by cells contributing to the repair process.

Within 16 hours of observation time, cells migrated toward the cell-free space (Figure 5A), and surprisingly, the overall wound closure on all three surfaces was in the range of 45 – 55% (**Figure S4**). We used software assisted analysis of the dynamic migratory behavior of cells on different substrates which gains insights into different dynamics of cell migration and is often applied when solely end-point measurement does not show significant differences. The trajectories of cells located within the cell-free gap are shown in Figure 5B. The analysis included dynamic investigation of mean migration speed (velocity) (Figure 5C) and mean number of neighbors (Figure 5D). The computer analysis revealed differences between the substrates in mean migration speed and mean number of neighbors. The values of the mean migration speed follow the order: TNT > TMS > Glass, which is adverse of the number of vinculin adhesion plaques per cell (Figure 4D). The mean migration speed on nanostructured titania is higher than on glass. The general trend of the mean speed decreases with time for all surfaces, most likely owed to the decrease in the cell-free gap area. The ability of cells to migrate is a response that is coupled with cell adhesion.[50] The stronger the cell adhesion is, the less migratory behavior the cell displays. Vinculin is necessary for binding cell surface integrin receptors to the ECM adhesion molecules, which in part controls the process of cell spreading and movement. It has been shown earlier that regular nanotopography reduces cell adhesion very markedly.[49] Dalby *et al*.[51] showed that nano-islands caused fibroblast adhesions to be smaller and less pronounced in comparison to large dash adhesions on flat substrates. Moreover, such features as ruffled lamellipodial protrusions and low number of

bundled long stress fibers are indicative of motile cells. It was suggested that the structure of F-actin can act as an indicator of more motile cells, which were in the process of forming and disassembling their focal adhesion (turn-over) required for migration. Similar results were reported by Brammer *et al*.,[52] where small dot adhesions were observed on TiO_2 nanotubes compared to large dash adhesions on flat titanium. Moreover, the cells cultured on TMS and glass have a higher number of neighboring cells (Figure 5C) that corresponds well to the cell area (Figure 4C).

Figure 6 depicts the cell-nanotopography interactions and corresponding effects on cell migratory behavior. Cells cultured on TMS and glass are larger and more spread, therefore having more opportunities to form cell-cell contacts. It has been appreciated that cells can adopt different modes of cell migration, either independent as single cells, or in close proximity and therefore communicative with their neighboring cells, forming close cell-cell contacts.[53] In comparison to single cell migration (TNT), collective cell migration is thought to support "supracellular" properties, such as collective polarization, force generation, decision making and, eventually, complex tissue organization (TMS).

3. Conclusion

The present study investigated the effect of ordered and disordered titania nanotopographies on the response of MC3T3-E1 cells such as cell proliferation, morphology, adhesion, and migration. We showed here that surface nanotopography affects cell properties. The cell morphology is affected by surface nanotopography: polygonal cell shape and spreading on mesoporous titania, elongated polarized shape (also elongated cell nuclei) on nanotubular titania. Control glass substrate has the similar effect as TMS; however, the cells are smaller and thinner. The effect of nanotopography on cell attachment and morphology observed at the early stages influences the density of the cells at later stages. Diminished cell adhesion on nanostructured surfaces has different reasons: the unfavorable density and localization of adsorbed protein preventing integrin clustering in case of TNT and very low contact angle in

case of TMS. Nanostructured titania surfaces induce distinct migratory behavior. The mean migration speed correlates with the strength of cell adhesion: the highest speed cells have on TNT. The mean number of neighboring cells correlates with the cell area: larger well spread cells on TMS and on glass have more neighbours than elongated cells on TNT. Each of the surfaces induces specific migratory behavior. The results of this study indicate that preosteoblasts respond differently on ordered and disordered nanotopography with altered morphology, adhesion and migration.

4. Experimental Section

Production of nanostructured surfaces: For the production of mesoporous titania (TMS) samples, a titanium layer (99.9%) of thickness 400 nm was deposited on glass substrates by means of Electron Beam Physical Vapor Deposition method (EB-PVD). TMS were obtained by sonochemical treatment with high intensity ultrasound (HIUS) in alkali solution. The size of the substrates was approx. 1 x 1 cm^2 to fit the homemade Teflon sample holder used for HIUS. Prior to sonication, the metal plates were degreased with isopropanol and rinsed with Milli-Q water (18 MΩ·cm). Titanium plates were ultrasonically treated in presence of 5M NaOH using the ultrasonic processor UIP1000hd (Hielscher Ultrasonics GmbH, Germany) with a maximum output power of 1000 W. The apparatus was equipped with a sonotrode BS2d18 (head area 2.5 cm^2) and booster B2-2.2, magnifying the working amplitude 2.2 times. Sonication was performed at *approximately* 20 kHz and constant temperature of around 333 K monitored by the thermo sensor inserted into the working solution.

For the production of titania nanotubes (TNT), titanium layer (99.9%) of thickness 400 nm was deposited on ITO-coated glass substrates by means of the Electron Beam Physical Vapor Deposition method (EB-PVD). TNTs were obtained by electrochemical oxidation. For their preparation, the Ti-ITO-glass samples were anodized in an aqueous solution of ethylene glycol (2 vol. % water) containing 0.75 wt. % NH_4F. At the beginning of the anodization, the potential was linearly increased from 0 to 40 V over a time of 5 minutes, then the anodization

was performed using the potentiostatic (40 V) mode till the total oxidation of a titanium layer on ITO.

All samples were additionally rinsed with ethanol and water and heat treated at 450 °C in the oven for at least 3 hours. Bulk titanium or its alloys, although being very tough, can be used for modification. In our experiments with cell studies it is advantageous to use a nanoscale-thick Ti layer on a glass substrate rather than bulk titanium, since the optical observation of the cell growth requires transparent samples. After thermal treatment, the titania layer on glass is transparent enough to observe cell adhesion and growth on the surface. As model, we use a 400 nm deposited layer on glass or on silicon for further atomic force microscopy study.

Milli-Q water (18 MΩ·cm) was used in all aqueous solutions. As a control glass substrates were used.

Physicochemical properties analysis: The specimen surface nanotopography was inspected by scanning electron microscopy (SEM; Gemini Leo 1550 instrument, Leo Elektronenmikroskopie GmbH, Germany) at an operating voltage of 3 keV. Surface roughness (R_a) and 3D roughness profiles of the surfaces were obtained with atomic force microscopy (AFM; Dimension, Bruker, Germany) and image analysis was performed with the Nanoscope V614r1 software. AFM measurements were carried out in air at room temperature in tapping mode with micro cantilevers OMCL-AC160TS-W (Olympus, Japan). Typical cantilever values: resonant frequency 300 kHz; spring constant 42 N/m. Atomic force micrographs of a scan size 3 x 3 μm were made on three different places on the sample. Contact angle was measured using the homemade system described in reference.[54]

Cell culture model: A mouse calvarial preosteoblast cell line MC3T3-E1 was obtained from Ludwig Boltzmann Institute, Vienna, Austria. Preosteoblasts were maintained in normal culture medium α-MEM, supplemented with 10% (by volume) fetal calf serum (FCS), 4500 mg glucose, 0.1% (by volume) gentamycin, 0.1% (by volume) ascorbic acid under standard culture condition (37°C, 5% CO_2 in a humidified atmosphere). Cells were passaged in total

three times every 24 hours by a dilution factor of 1/6. The media was refreshed every 48 h. After reaching confluence, cells were dissociated from culture vessels by incubating with pronase for 3 – 5 min. All surfaces and scaffolds were autoclaved before cell culture experiments.

Cell attachment: Up to 30 optical images of each sample were captured after 3 and 24 hours of growth with the Phase Contrast Microscope (Nikon Eclipse TS100, Japan) equipped with a digital camera (Nikon Digital sight DS 2Mv). The statistical analysis of the cell attachment on different substrates was obtained using image analysis software Image J (version 1.47). The threshold is set between 30 and 40 (out of 255). The software automatically detects the cell outline and calculates parameters such as the number of cells per unit area (cell density, [cells·mm^{-2}]) and cell area per unit area of the substrate (cell coverage, [%]).[55-56]

Cell morphology: Morphologies of MC3T3-E1 cells cultured on various surfaces were observed by confocal laser scanning microscopy (CLSM) and SEM. The cells were seeded onto surfaces at a density of 6000 cells·cm^{-2}. Normal culture medium and standard conditions were employed. At respective time point after seeding, the cells were washed twice with phosphate-buffered saline (PBS). To prepare samples for CLSM observation, the cells were fixed with 4% paraformaldehyde in PBS, and permeabilized with buffered Triton-X100 (Sigma-Aldrich, Steinheim, Germany) for 10 min at room temperature. The scaffolds were then thoroughly washed with PBS and stained for 60-90 min with phalloidin Alexa488 (Invitrogen, Oregon, USA) (1:20) in dark at 4°C for cytoskeletal filamentous F-actin. After that scaffolds were thoroughly washed with PBS again, and stained for nuclei with TO-PRO3 iodide (Invitrogen, Oregon, USA) (1:300) for 5 min at room temperature. The scaffolds were washed with PBS, mounted with Fluoro-Mount in inverted position on the glass slides, and examined via confocal microscopy (Leica Microsystems, Mannheim, Germany).

To prepare samples for SEM observation, the cells were fixed twice: primary fixation with 2.5% glutaraldehyde (in PBS) for 30 min and secondary fixation with 4% PFA for 20 min.

Thereafter, the cells were dehydrated by gradient ethanol solutions (25%, 50%, 75%, 90% and 100%), each for 5 min. The treated samples were dried overnight in desiccator, sputter-coated with gold and observed using SEM.

Cell adhesion: MC3T3-E1 cells were seeded onto surfaces maintaining the seeding density and culture method as described above. Cell adhesion was evaluated by immunofluorescent staining of focal contacts. At 3 hours after seeding, cells were fixed with 4% paraformaldehyde in PBS, quenched for 5 min in 50 mM ammonium chloride and permeabilized with buffered Triton-X-100 solution for 10 min. Specimens were then thoroughly washed with PBS and blocked in 3% BSA (in PBS) for 1 hour. After that samples were incubated overnight with anti-vinculin antibody (Sigma V9131) (1:300 in PBS/BSA). After washing with PBS, samples were incubated with secondary goat anti-mouse antibody Alexa594 (Invitrogen) (1:300) for 1 hour. After washing, samples were stained for 20 min with phalloidin Alexa488 (Invitrogen) (1:100). The staining was performed at room temperature, except for the incubation with anti-vinculin antibody overnight, when the samples were left at 4°C. The stained samples were mounted with Fluoro-Mount in inverted position on thin glass slides and examined via confocal microscopy. Imaging was conducted by using a Leica confocal laser scanning microscope (Leica Microsystems, Mannheim, Germany). The samples were excited with the argon laser line at 488 nm and 594 nm for Phalloidin Alexa488 (actin stain) and Alexa594 (focal contacts stain), respectively. The images were captured with a PL FLUOTAR objective.

Cell migration: In order to investigate migration characteristics of MC3T3-E1 cells, the wound healing assay was performed using ibidi Culture-Inserts (Ibidi GmbH, Germany) according to the manufacturer's instructions. MC3T3-E1 cells were seeded to become confluent in 10% FCS α-MEM. 1 hour prior to insert removal, cells were incubated with 10 μg/ml mitomycin C to block cell proliferation. After insert removal, the wound closure was allowed to proceed and imaged by phase contrast microscopy. Pictures were taken using a 5×

objective in bright field modus every 30 min for at least 16 h. Life cell imaging was performed within a heat and CO_2 controlled Life Cell Imaging chamber (ibidi GmbH) using an automated sample table mounted on an Axiovert 200 M (Carl Zeiss, Jena, Germany) in combination with Axiovision Mark&Find tool.

The cell migration analysis was performed with an automatic algorithm originally developed for cell migration analysis in chemotaxis assays. This approach allows estimating migration characteristics such as mean migration speed, neighborhood analysis, and is able to distinguish between directed and random migration without a favored direction. In brief, the automatic tracking algorithm includes two main steps: segmentation and tracking. Firstly, the dense optical flow is computed to segment the foregrounds which are the cells. The cell nuclei are roughly segmented by an adaptive inverse threshold, and the cell bodies are approximated from the nuclei via watershed segmentation on the foreground mask. Thus, the position and the neighborhood are computed for each cell at each time point on time-lapse data. The neighborhood is here defined as cells with adjacent voronoi areas. The trajectories are computed by an overlap heuristic on the nuclei mask. The analysis was restricted on cells close to the scratch area.

Image processing: For quantification of focal contacts, confocal microscopy images were as well analyzed using ImageJ 1.47 (**Figure S4**). In all of the samples, a minimum of 5 individual cells were analyzed. Each image was firstly spatially calibrated and converted to grayscale 8-bit images. After that the individual cell outlines were manually traced and the threshold intensity ranges were set at 65-255 as described earlier.[55, 57] And finally, the size parameters of the vinculin plaques were set between 0 and 6 μm^2 and number and area of the plaques were counted by the software. Up to 20 confocal planes were captured along the z-axis in order to perform 3D reconstructions and estimate the cell thickness. ImageJ 1.47 was then used to process the data and generate the 3D reconstruction.

The cell migration analyses were performed using Python 2.7.6 with the image processing libraries OpenCV 3.0.0 and scikit-image 0.12.3.

Statistical analysis: The data is expressed as mean ± standard deviation (SD) from at least three independent experiments (samples in triplicate). The statistical significance of differences in means was determined by one-way analysis of variance (ANOVA) with Origin 2015. The values of $p<0.001$ were considered as statistically significant.

5. Acknowledgements

The authors gratefully acknowledge the assistance from Anneliese Heilig in AFM measurements, Rona Pitschke and Heike Runge for performing SEM, Christine Pilz-Allen in assistance with cell culture maintenance, and Olga Baidukova for assistance with CLSM. The authors thank Dr. Daria V. Andreeva, PC II Bayreuth University, for the help with organization of vacuum deposition of titanium layers on different substrates. The authors are also grateful for all advices of Prof. Helmuth Möhwald.

References

[1] J. K. Mouw, G. Ou, V. M. Weaver, *Nat. Rev. Mol. Cell Biol.* **2014**, *15*, 771.
[2] D. Hubmacher, S. S. Apte, *Curr. Opin. Rheumatol.* **2013**, *25*, 65.
[3] F. Gattazzo, A. Urciuolo, P. Bonaldo, *Biochim. Biophys. Acta, Gen. Subj.* **2014**, *1840*, 2506.
[4] D. Karazisis, A. M. Ballo, S. Petronis, H. Agheli, L. Emanuelsson, P. Thomsen, O. Omar, *Int. J. Nanomed.* **2016**, *11*, 1367.
[5] M. Kulkarni, A. Mazare, E. Gongadze, S. Perutkova, V. Kralj-Iglic, I. Milosev, P. Schmuki, A. Iglic, M. Mozetic, *Nanotechnology* **2015**, *26*, 062002.
[6] H. N. Kim, A. Jiao, N. S. Hwang, M. S. Kim, D. H. Kang, D. H. Kim, K. Y. Suh, *Adv. Drug Delivery Rev.* **2013**, *65*, 536.
[7] C. Selhuber-Unkel, T. Erdmann, M. López-García, H. Kessler, U. S. Schwarz, J. P. Spatz, *Biophys. J.* **2010**, *98*, 543.
[8] E. A. Cavalcanti-Adam, T. Volberg, A. Micoulet, H. Kessler, B. Geiger, J. P. Spatz, *Biophys. J.* **2007**, *92*, 2964.
[9] S. Oh, K. S. Brammer, Y. S. J. Li, D. Teng, A. J. Engler, S. Chien, S. Jin, *Proc. Natl. Acad. Sci. U. S. A.* **2009**, 10.1073/pnas.0813200106.
[10] B. Trappmann, J. E. Gautrot, J. T. Connelly, D. G. T. Strange, Y. Li, M. L. Oyen, M. A. Cohen Stuart, H. Boehm, B. Li, V. Vogel, J. P. Spatz, F. M. Watt, W. T. S. Huck, *Nat. Mater.* **2012**, *11*, 642.
[11] E. Cukierman, R. Pankov, K. M. Yamada, *Curr. Opin. Cell Biol.* **2002**, *14*, 633.
[12] M. J. Dalby, N. Gadegaard, R. O. C. Oreffo, *Nat. Mater.* **2014**, *13*, 558.
[13] F. Variola, J. Brunski, G. Orsini, P. T. de Oliveira, R. Wazen, A. Nanci, *Nanoscale* **2011**, *3*, 335.

[14] X. Liu, P. K. Chu, C. Ding, *Mater. Sci. Eng., R* **2004**, *47*, 49.
[15] A. M. Ballo, A. Palmquist, O. Omar, W. Xia, *Dental Implant Surfaces - Physicochemical Properties, Biological Performance, and Trends*, INTECH Open Access Publisher, 2011.
[16] F. Variola, F. Vetrone, L. Richert, P. Jedrzejowski, J.-H. Yi, S. Zalzal, S. Clair, A. Sarkissian, D. F. Perepichka, J. D. Wuest, F. Rosei, A. Nanci, *Small* **2009**, *5*, 996.
[17] J. Banhart, *Prog. Mater Sci.* **2001**, *46*, 559.
[18] S. Amin Yavari, J. van der Stok, Y. C. Chai, R. Wauthle, Z. Tahmasebi Birgani, P. Habibovic, M. Mulier, J. Schrooten, H. Weinans, A. A. Zadpoor, *Biomaterials* **2014**, *35*, 6172.
[19] R. A. Gittens, R. Olivares-Navarrete, A. Cheng, D. M. Anderson, T. McLachlan, I. Stephan, J. Geis-Gerstorfer, K. H. Sandhage, A. G. Fedorov, F. Rupp, B. D. Boyan, R. Tannenbaum, Z. Schwartz, *Acta Biomater.* **2013**, *9*, 6268.
[20] S. Dey, M. Das, V. K. Balla, *Mater. Sci. Eng., C* **2014**, *39*, 336.
[21] C.-M. Han, H.-E. Kim, Y.-H. Koh, *Surf. Coat. Technol.* **2014**, *251*, 226.
[22] N. Faucheux, R. Schweiss, K. Lützow, C. Werner, T. Groth, *Biomaterials* **2004**, *25*, 2721.
[23] P. J. ter Brugge, J. G. Wolke, J. A. Jansen, *J. Biomed. Mater. Res.* **2002**, *60*, 70.
[24] E. Anitua, R. Prado, G. Orive, R. Tejero, *J. Biomed. Mater. Res., Part A* **2015**, *103*, 969.
[25] S. Bauer, P. Schmuki, K. von der Mark, J. Park, *Prog. Mater Sci.* **2013**, *58*, 261.
[26] K. von der Mark, J. Park, *Prog. Mater Sci.* **2013**, *58*, 327.
[27] Y. Zhukova, S. A. Ulasevich, J. W. C. Dunlop, P. Fratzl, H. Möhwald, E. V. Skorb, *Ultrason. Sonochem.* **2016**.
[28] D. V. Andreeva, D. V. Sviridov, A. Masic, H. Möhwald, E. V. Skorb, *Small* **2012**, *8*, 820.
[29] J. Kopf, S. Ulasevich, O. Baidukova, Y. Zhukova, J. W. C. Dunlop, P. Fratzl, P. Rikeit, P. Knaus, S. K. Poznyak, D. V. Andreeva, E. V. Skorb, *Adv. Eng. Mater.* **2016**, *18*, 476.
[30] A. Ghicov, P. Schmuki, *Chem. Commun.* **2009**, 10.1039/b822726h, 2791.
[31] E. A. Vogler, *Adv. Colloid Interface Sci.* **1998**, *74*, 69.
[32] M. J. P. Biggs, R. G. Richards, M. J. Dalby, *Nanomedicine: Nanotechnology, Biology, and Medicine* **2010**, *6*, 619.
[33] J. Park, S. Bauer, K. von der Mark, P. Schmuki, *Nano Lett.* **2007**, *7*, 1686.
[34] A. J. Ridley, M. A. Schwartz, K. Burridge, R. A. Firtel, M. H. Ginsberg, G. Borisy, J. T. Parsons, A. R. Horwitz, *Science* **2003**, *302*, 1704.
[35] C. Le Clainche, M.-F. Carlier, *Physiol. Rev.* **2008**, *88*, 489.
[36] R. You, X. Li, Y. Liu, G. Liu, S. Lu, M. Li, *J. Biomed. Mater. Res., Part A* **2014**, *102*, 4206.
[37] S. D. Puckett, P. P. Lee, D. M. Ciombor, R. K. Aaron, T. J. Webster, *Acta Biomater.* **2010**, *6*, 2352.
[38] S. Lavenus, D. J. Poxson, N. Ogievetsky, J. S. Dordick, R. W. Siegel, *Biomaterials* **2015**, *55*, 96.
[39] O. Zinger, K. Anselme, A. Denzer, P. Habersetzer, M. Wieland, J. Jeanfils, P. Hardouin, D. Landolt, *Biomaterials* **2004**, *25*, 2695.
[40] J. Zhou, Y. Han, S. Lu, *Int. J. Nanomed.* **2014**, *9*, 1243.
[41] R. Zhang, H. Wu, J. Ni, C. Zhao, Y. Chen, C. Zheng, X. Zhang, *Mater. Sci. Eng., C* **2015**, *53*, 272.
[42] K. S. Brammer, S. Oh, C. J. Cobb, L. M. Bjursten, H. v. d. Heyde, S. Jin, *Acta Biomater.* **2009**, *5*, 3215.
[43] A. Buxboim, I. L. Ivanovska, D. E. Discher, *J. Cell Sci.* **2010**, *123*, 297.
[44] M. T. Yang, N. J. Sniadecki, C. S. Chen, *Adv. Mater.* **2007**, *19*, 3119.

[45] M. J. P. Biggs, R. G. Richards, N. Gadegaard, C. D. W. Wilkinson, M. J. Dalby, *J. Mater. Sci.: Mater. Med.* **2007**, *18*, 399.
[46] A. S. G. Curtis, N. Gadegaard, M. J. Dalby, M. O. Riehle, C. D. W. Wilkinson, G. Aitchison, *IEEE Transactions on NanoBioscience* **2004**, *3*, 61.
[47] M. J. Dalby, N. Gadegaard, M. O. Riehle, C. D. W. Wilkinson, A. S. G. Curtis, *Int. J. Biochem. Cell Biol.* **2004**, *36*, 2005.
[48] E. A. Cavalcanti-Adam, D. Aydin, V. C. Hirschfeld-Warneken, J. P. Spatz, *HFSP J.* **2008**, *2*, 276.
[49] A. S. G. Curtis, B. Casey, J. O. Gallagher, D. Pasqui, M. A. Wood, C. D. W. Wilkinson, *Biophys. Chem.* **2001**, *94*, 275.
[50] E. Scarpa, R. Mayor, *J. Cell Biol.* **2016**, *212*, 143.
[51] M. J. Dalby, M. O. Riehle, H. Johnstone, S. Affrossman, A. S. G. Curtis, *Biomaterials* **2002**, *23*, 2945.
[52] K. S. Brammer, S. Oh, J. O. Gallagher, S. Jin, *Nano Lett.* **2008**, *8*, 786.
[53] P. Friedl, D. Gilmour, *Nat Rev Mol Cell Biol* **2009**, *10*, 445.
[54] S. Karpitschka, H. Riegler, *Langmuir* **2010**, *26*, 11823.
[55] M. A. Woodruff, P. Jones, D. Farrar, D. M. Grant, C. A. Scotchford, *J. Mol. Histol.* **2007**, *38*, 491.
[56] H. Chen, W. Song, F. Zhou, Z. Wu, H. Huang, J. Zhang, Q. Lin, B. Yang, *Colloids Surf., B* **2009**, *71*, 275.
[57] M. K. Strulson, D. M. Johnson, J. A. Maurer, *Langmuir* **2012**, *28*, 4318.

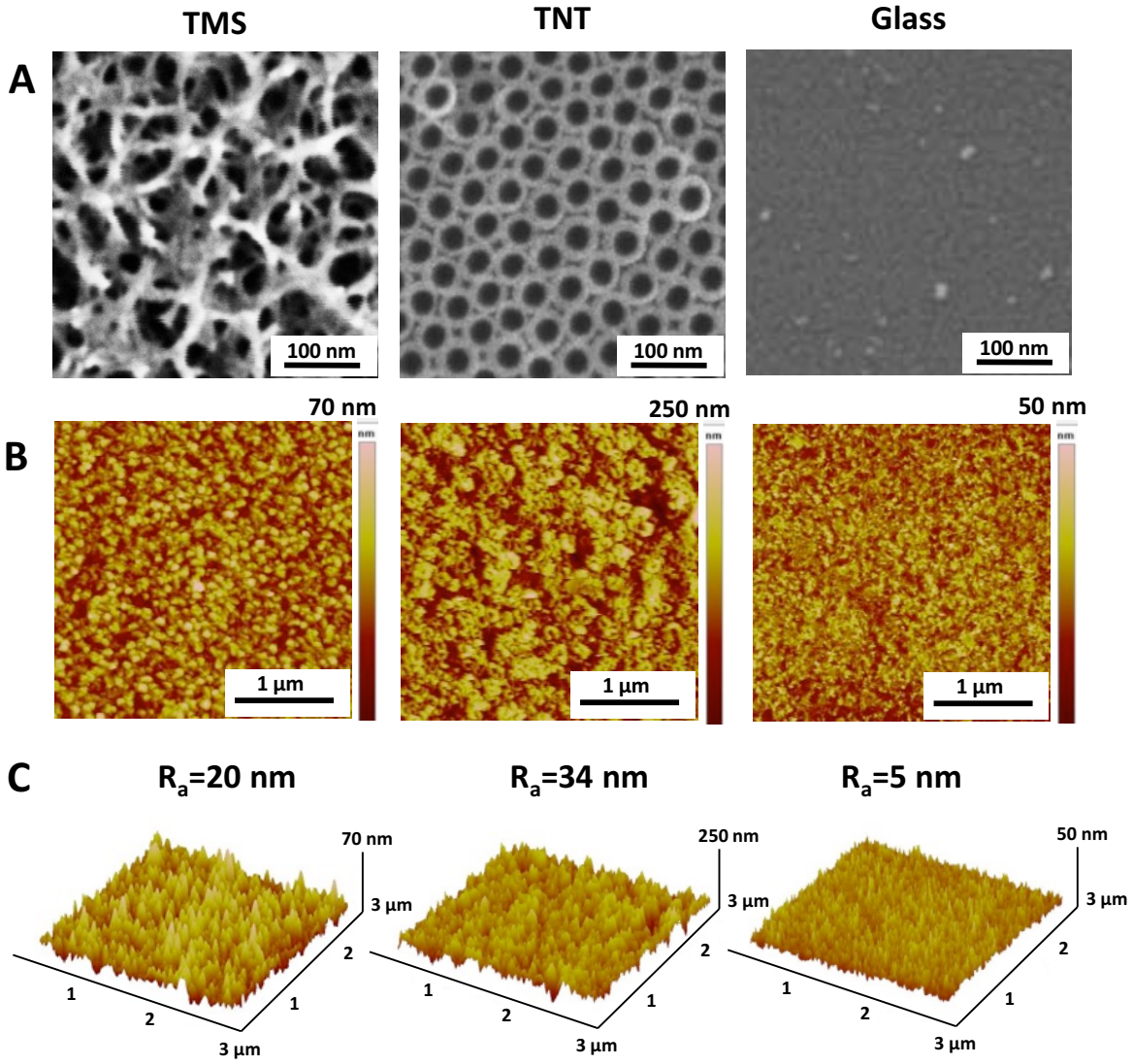

Figure 1. Physicochemical surface characterization: SEM micrographs (A), AFM height images (B), and 3D roughness profiles (C) of titania surfaces. SEM reveals disordered pores inhomogeneous in size and shape of mesoporous titanium and vertically oriented pores of nanotubes with average diameter of approx. 70 nm. TMS and TNT have shown average image roughness of *approximately* 20 and 30 nm, respectively. The average image roughness (Img. R_a) was calculated from the images taken at three different places on the surface.

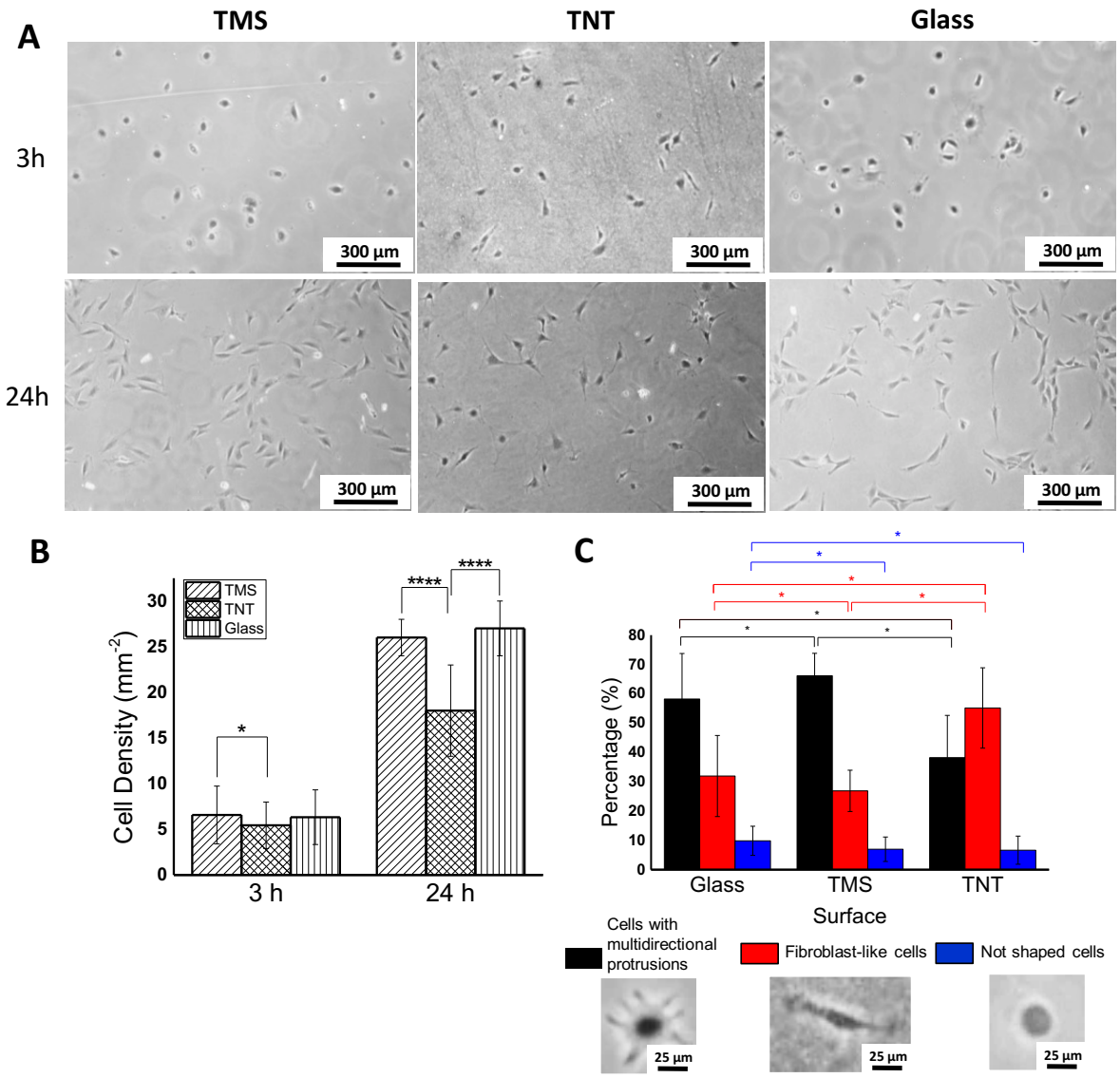

Figure 2. Cell proliferation analysis: Optical images of MC3T3-E1 cells after 3 and 24 hours (A) upon seeding on titania surfaces. MC3T3-E1 cell densities on different substrates (B) and analysis of MC3T3-E1 cell shape after 3 hours (C). Error bars represent standard deviation. Three samples were tested per substrate type; three independent experiments were conducted. * indicates $p < 0.001$; **** indicates $p < 0.05$.

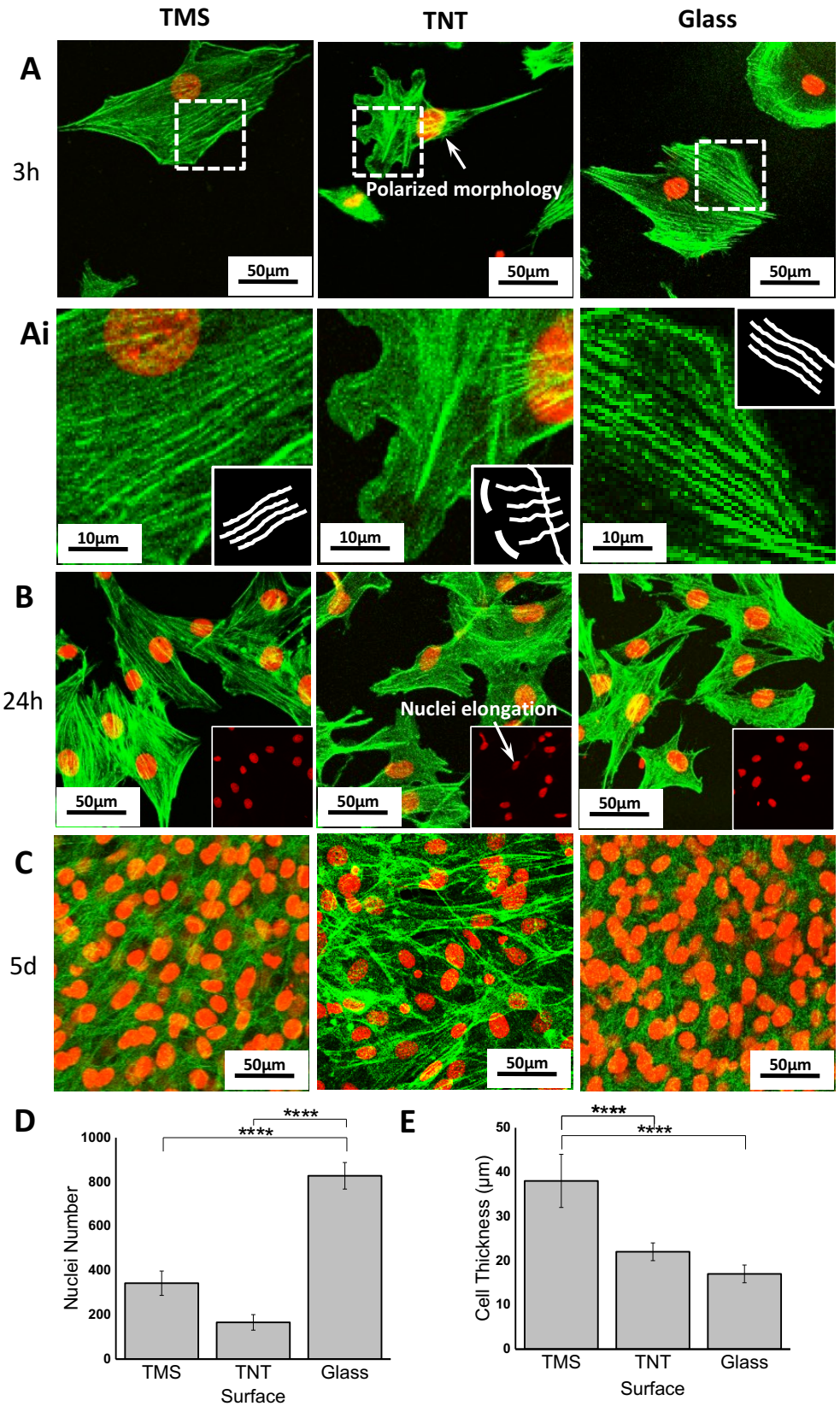

Figure 3. Cell morphology analysis: Actin (green) and cell nucleus (red) fluorescence images of MC3T3-E1 cells cultured on titania surfaces for 3 hours (A), 24 hours (B), and 5 days (C). Offsets on (Ai) show actin alignment. Cell thickness after 3 hours of growth (D).Number of cell nuclei calculated after 5 days of tissue growth (E).

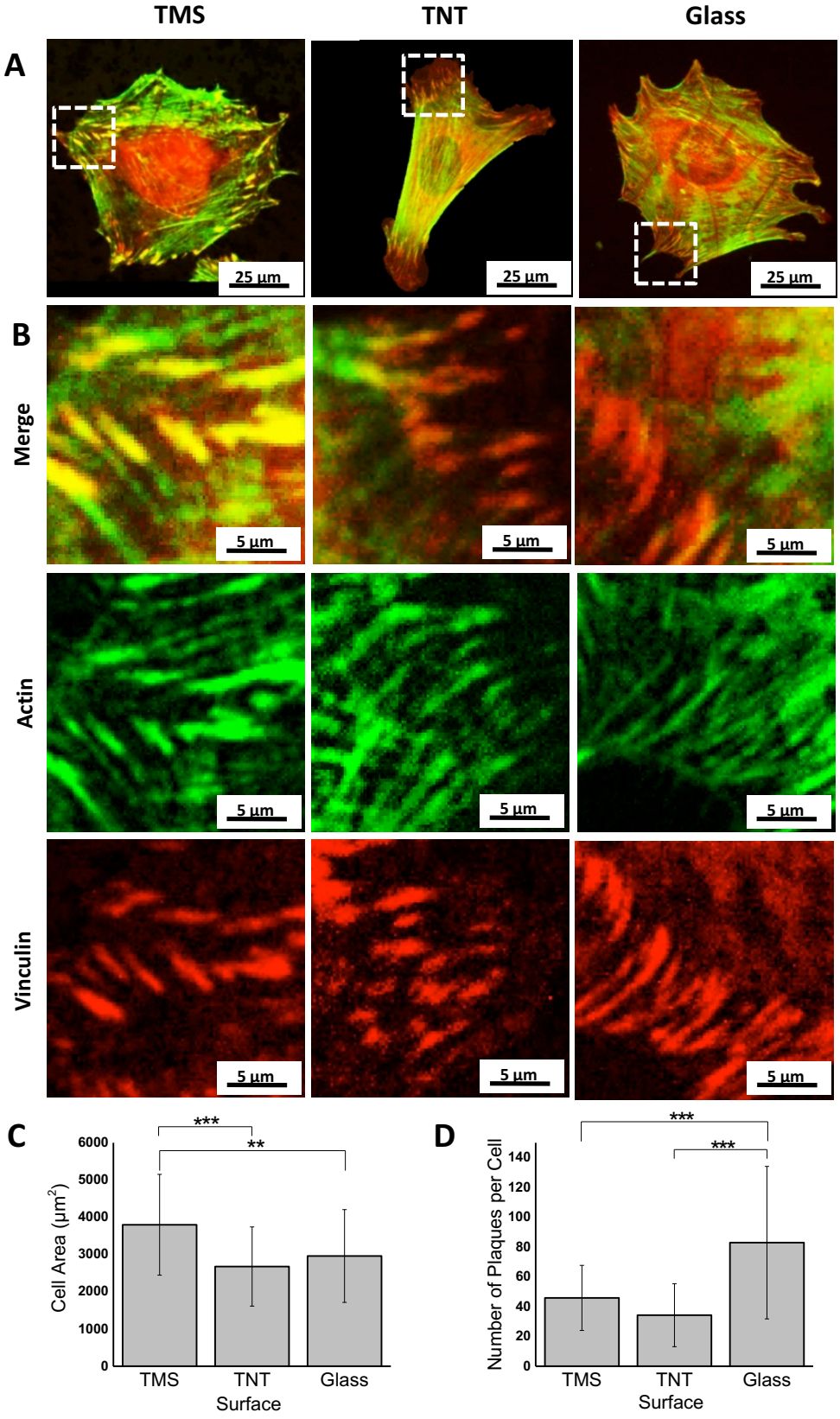

Figure 4. Cell adhesion analysis: Confocal microscopy images with actin (green) and vinculin (red) staining showing MC3T3-E1 cell adhesion on the substrates after 3 hours (A). Magnified images of focal contact points (B). Average cell area (C) and average number of vinculin adhesion plaques per one cell (D) at 3 hours. Error bars represent standard deviation.

Three samples were tested per substrate type; three independent experiments were conducted. ** indicates $p < 0.005$; *** indicates $p < 0.01$.

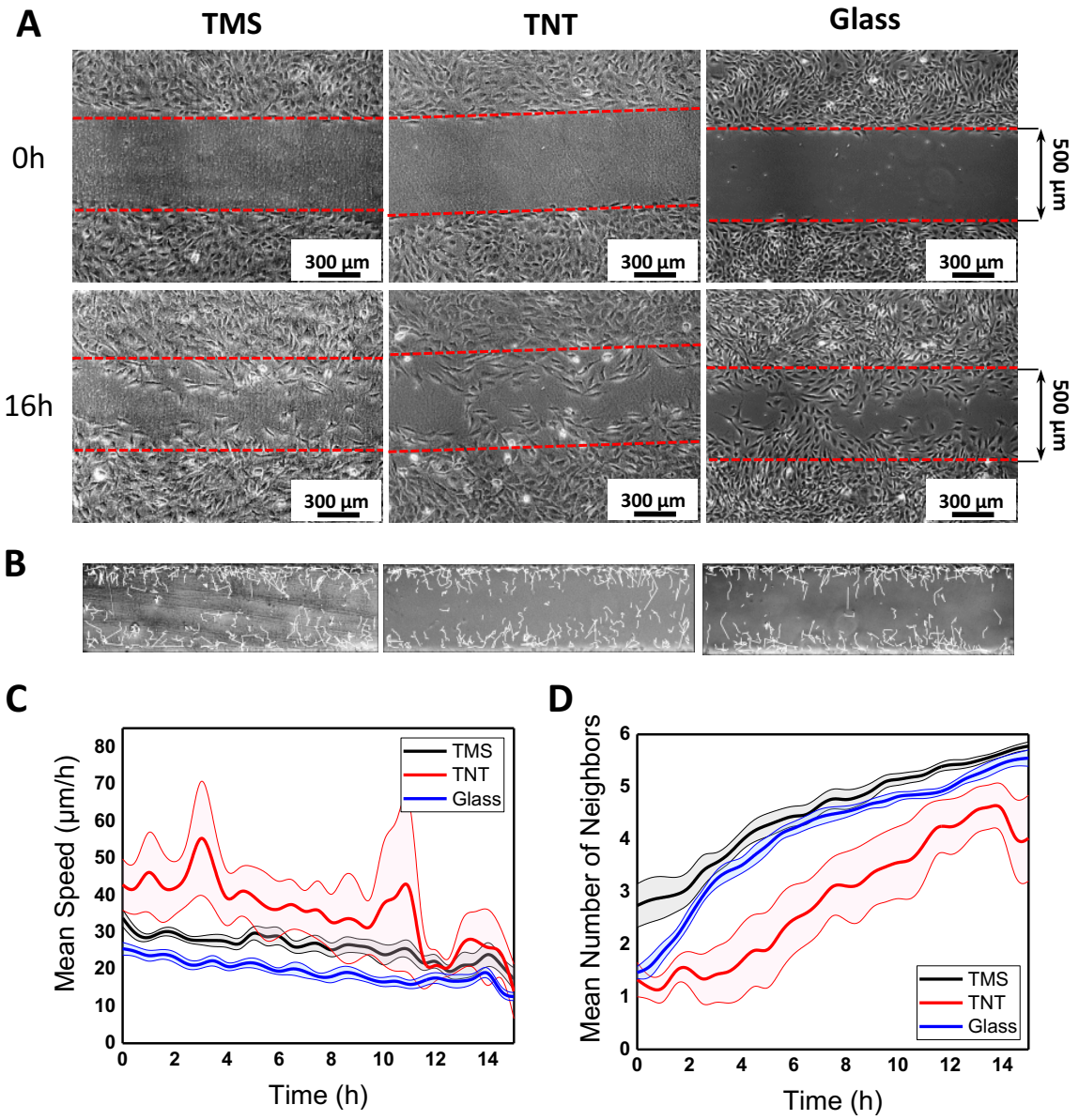

Figure 5. Cell migration analysis: Wound healing assay of MC3T3-E1 preosteoblast cell line on titania surfaces in presence of the proliferation inhibiting factor Mitomycin C (10µg/ml) (A). α-MEM Cell culture medium was supplemented with 10% FCS. Live cell imaging was monitored for 16 hours. Cell trajectories within cell-free gap (B). Mean migration speed (C). Line in bold depicts the mean value, highlighted area depicts standard error of the mean (±SEM). Neighborhood analysis of migrating cells: the mean number of neighboring cells for each time step (D). Shown is the mean over three independent experiments for each substrate group (glass, TMS, TNT).

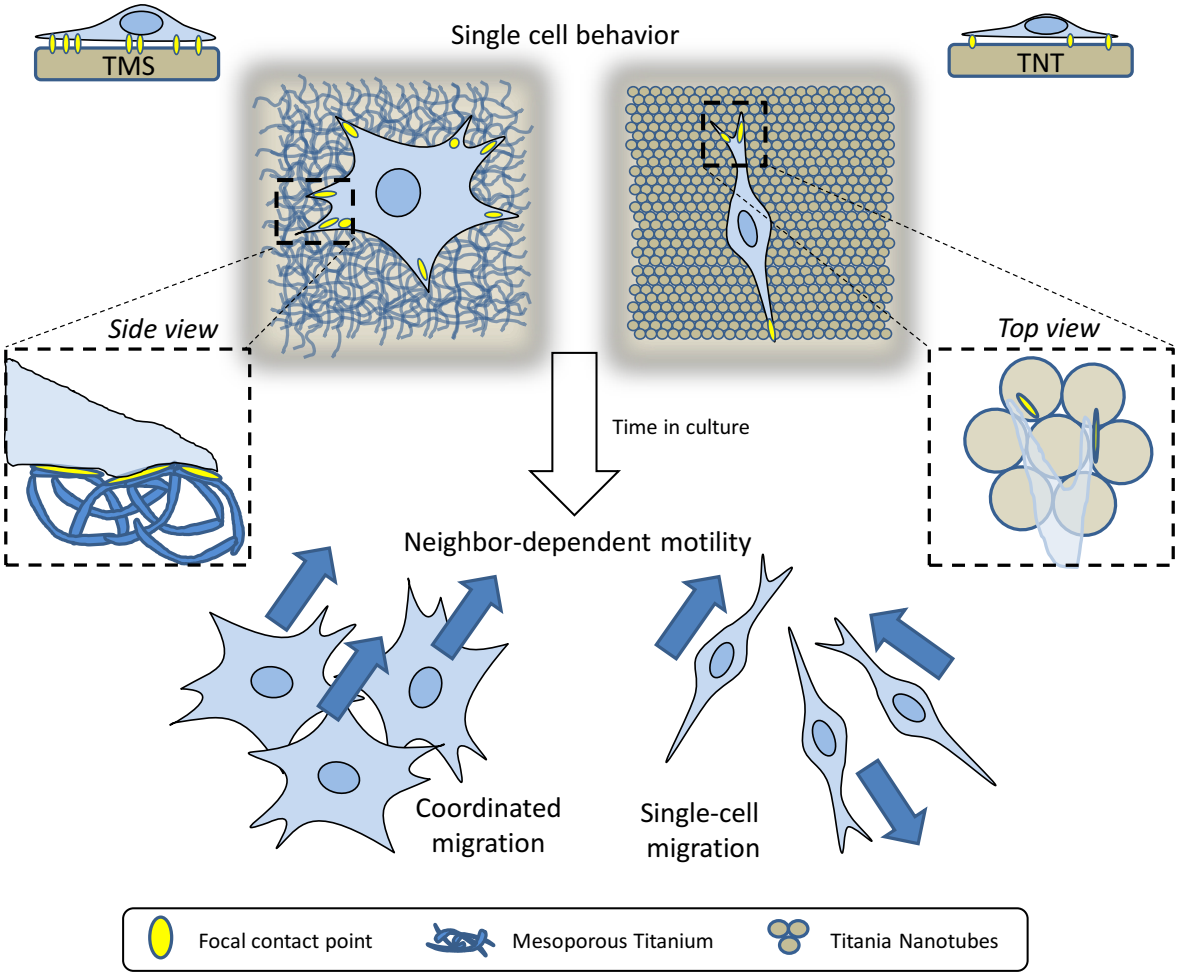

Figure 6. Cell behavior on mesoporous and nanotubular titania surfaces.

Supporting Information

The role of surface nanotopography on preosteoblast morphology, adhesion and migration

Yulia Zhukova, Christian Hiepen, Petra Knaus, Marc Osterland, Steffen Prohaska, John W. C. Dunlop, Ekaterina V. Skorb, Peter Fratzl

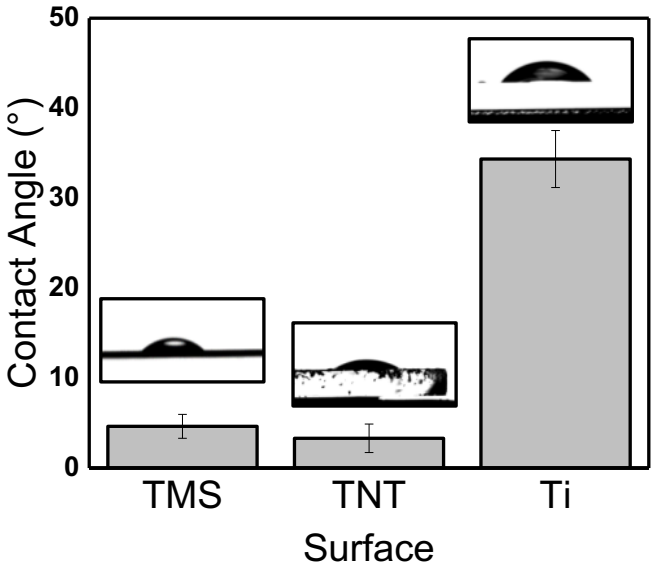

Figure S1. Surface wettability of various surfaces.

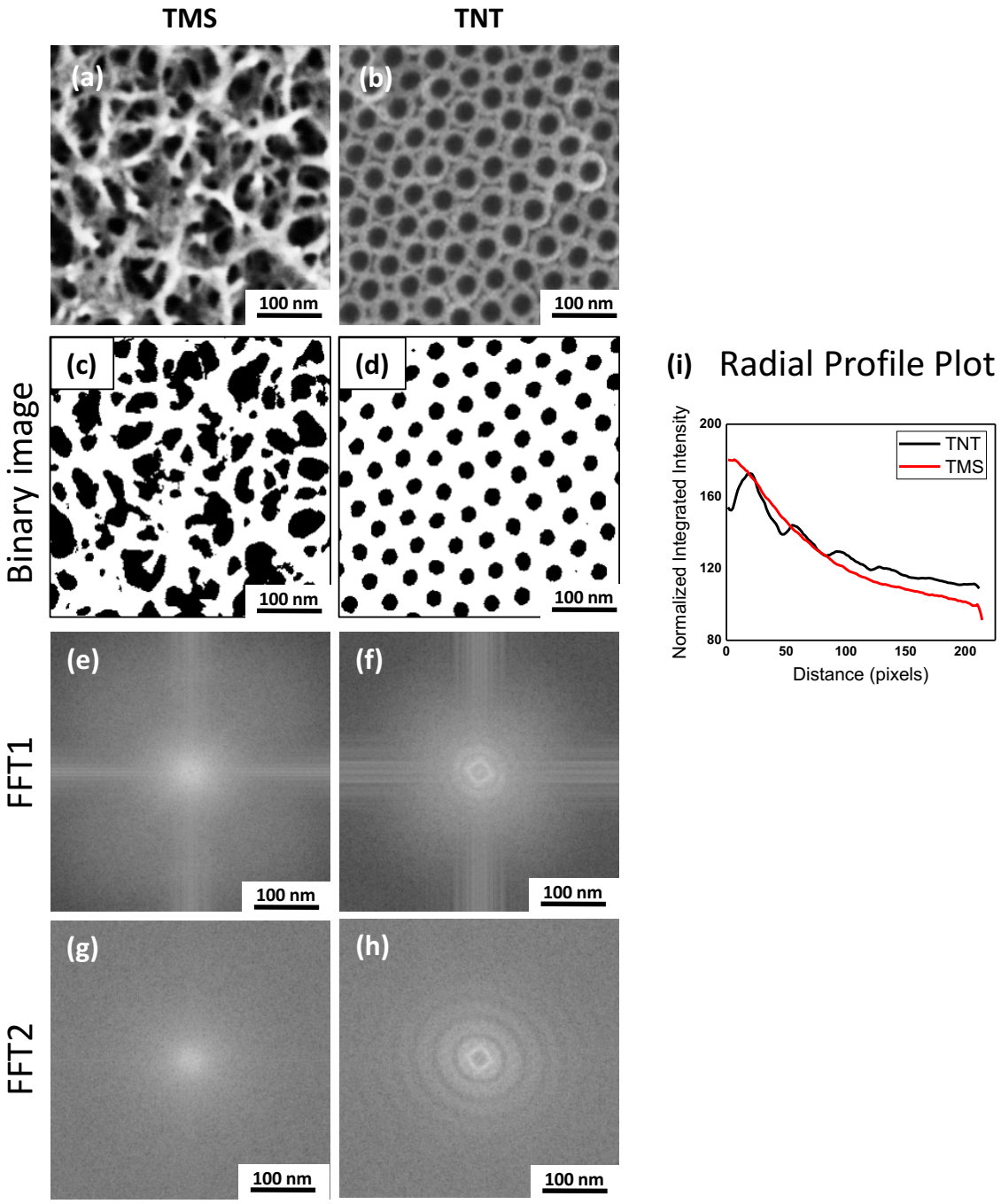

Figure S2. Fast Fourier Transform (FFT) measurements to estimate the level of nanotopography disorder. SEM micrographs of mesoporous and nanotubular titania surfaces (a-b) were firstly binarized (c-d), and then FFT measurement was performed twice (e-h), followed by the radial integration of the processed image, resulting in a radial profile plot (i) of the nanotopographies.

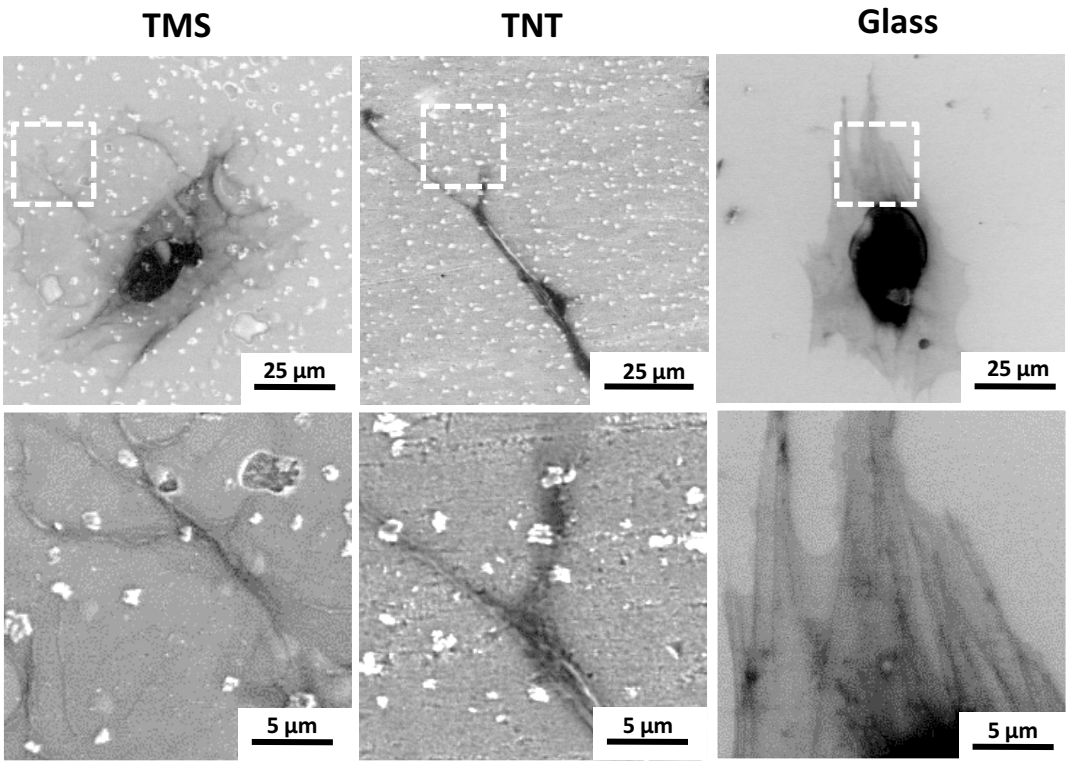

Figure S3. SEM micrographs of MC3T3-E1 cells cultured on various surfaces for 24 hours.

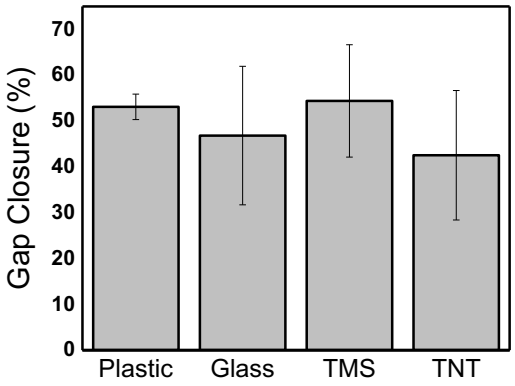

Figure S4. Gap closure values obtained from the wound healing assay of MC3T3-E1 preosteoblast cell line on titania surfaces in presence of the proliferation inhibiting factor Mitomycin C (10µg/ml). α-MEM Cell culture medium was supplemented with 10% FCS.

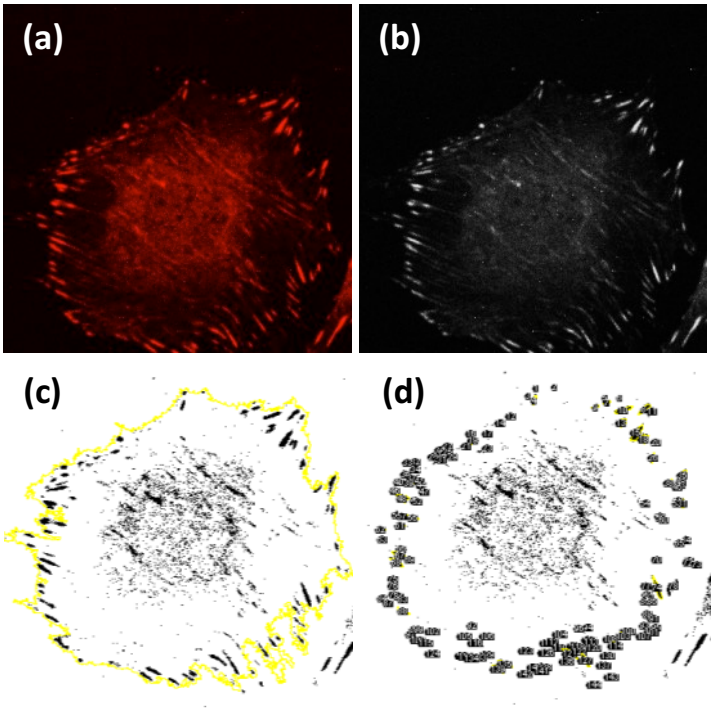

Figure S5. Process of cell area and focal contact quantification. Initial confocal microscopy micrograph (a). Conversion to greyscale 8-bit image and cell outline tracing (b). Intensity threshold adjustment (c). Vinculin plaques counted based on their size parameters (d).